Setting-up rules to characterize microsegregation

A Hazotte, J.S. Lecomte, Jacques Lacaze

Setting-up rules to characterize microsegregation

A. Hazotte [a], J.S. Lecomte [a], J. Lacaze [b,*]

[a] *LETAM, UMR no. 7078, Université Paul-Verlaine, Metz, Ile du Saulcy, France*

[b] *CIRIMAT, ENSIACET, UMR no 5085, 31077 Toulouse Cedex 4, France*

∗ Corresponding author. Tel.: +33 5 62 88 57 10; fax: +33 5 62 88 56 63.
E-mail address: jacques.lacaze@ensiacet.fr (J. Lacaze).

Abstract

Characterization of chemical heterogeneities such as microsegregation resulting from solidification of metallic alloys is most often performed by EDS or WDS microanalysis with spot measurements located at corners of a regular grid. Rather than attempting a theoretical treatment of the statistics of such analyses, the quality of the procedure has been investigated by implementing "measurement" grids on numerical images that mimic solidification structures. Microstructures either with no geometrical constraints (uniform distribution of the solid nuclei) or with limited constraints that give some periodicity have been investigated. Systematic analysis of the effect of the location and size of the "measurement" grid enlightens the procedures which should be followed to minimize bias.

Keywords: Solidification; Microsegregation; Image analysis; Solute distribution

1. Introduction

Chemical heterogeneities build-up during casting and solidification of metallic alloys. They mainly result from limited cooling rate which inhibits solid-state diffusion, although solute redistribution at dendrite tips as well as kinetics undercooling of eutectics may also affect them [1]. These so-called microsegregations are of first importance for net-shape castings, as well as for semi-finished parts or for weldings (see for instance [2] for a review).

The first obvious evidence of microsegregation is the presence of a second (eutectic) phase in alloys which should be single phase according to the phase diagram. Thus, the first attempts of quantifying the level of heterogeneities in a cast alloy were performed by measuring the amount of eutectic or second phase [3]. The development of microprobe analysis led to the definition of segregation indexes which are still in use [4]. However, the capabilities of microanalysers to be automated suggested performing extensive analyses that may give information not only on the second phase(s) but also on the matrix. This is particularly important when interest is put not only on solidification but also on subsequent solid-state transformations [5,6].

The most usual way of characterizing microsegregation is to perform successive measurements in spot mode (say with a probe diameter of 1 _m) at regular intervals along lines or grids. This method was first proposed by Flemings [4] using a nonautomatic microprobe, then extended by Feest and Doherty [7] when automatic stages became available. Since then, numerous studies made use of this method. However, although automatic, it remains time consuming and data collection does therefore generally not exceed 400–600 measurements obtained through overnight sessions using either wavelength dispersive spectrometry (WDS) or energy dispersive spectrometry (EDS) analysis. Such a number is usually implicitly considered as 'sufficient' if dealing with the estimation of second phase(s) amount, while the statistical confidence ranges are rarely discussed when concerned with the estimation and comparison of chemical composition distribution(s). As a matter of fact, this latter

analysis is difficult since the measurement points are in most cases correlated due to the fact that lines or grids usually scan a small area with respect to the characteristic size of the solidification microstructure. To the best of knowledge of the authors, the problem of statistic validity of experimental composition distributions obtained by this method has been considered only by Gungor [8], who attempted to apply classical statistics, and by Yang et al. [9], who discussed their experimental results with regard to random sampling data recorded on highly regular simulated structures.

Through an approach of the latter type, the present paper points out the statistical bias which can result from chemical analyses along regular grids and proposes some rules to minimize them. Firstly, different algorithms will be used to simulate more or less 'realistic' chemical composition maps (images) with a composition distribution based on a classical solidification model. Then, results of 'grid' analyses performed with different 'experimental' (sub-sampling) conditions will be compared to this reference distribution and the differences will be stressed. The discussion will lastly propose some ways of optimizing the analysis procedure. In this preliminary work, only 2D images and binary alloys from a simple eutectic system are considered.

2. Simulation of "chemical" images

2D composition images of a binary alloy were created by firstly implementing seeds of solid, then making them grow into a matrix representing the liquid. Solidification was assumed to follow Scheil's model according to which the composition ω^s(all compositions given as weight content) of the solid which deposits in case of single-phase precipitation is given as

$$\omega^s = k\,\omega^0(1-f^s)^{k-1} \qquad (1)$$

where ω^0 is the nominal solute content of the alloy, f^s the actual solid fraction and k is the solute partition coefficient between solid and liquid ($k = \omega^s/\omega^0$), assumed to remain constant over the whole solidification range. Solidification ends on a eutectic with an average homogeneous composition given by the phase diagram. The data used in the following were inspired by the Al–Cu phase diagram and we set ω^0 = 0.04, k = 0.17 and ω^{eut} = 0.33. According to the Scheil's model, the expected weight fraction of eutectic is f^{eut} ≈8%. It will be considered that solid and liquid phases have the same density so that weight and volume fractions are equal. The maximum solubility of Cu in the matrix is obtained when the eutectic is reached, it is kω^{eut} = 0.056.

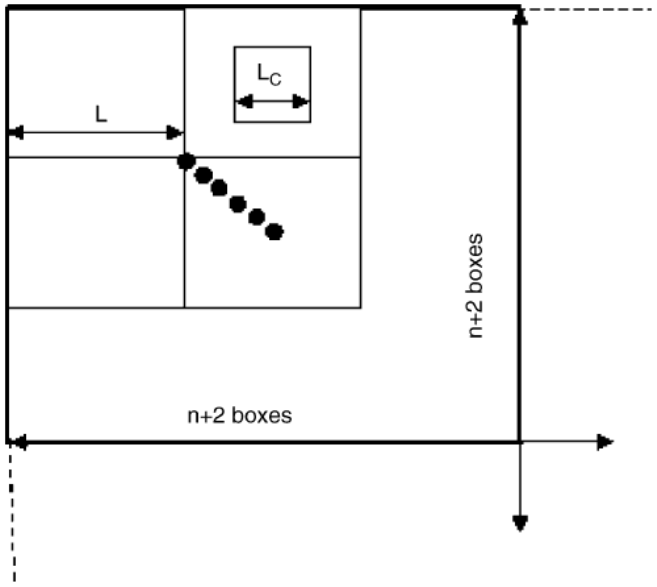

Fig. 1. Schematic showing how are implemented the boxes and the areas for seeding in the case of non-random patterns. Dots represent the location of the first point for analysis with a grid having a step equal to the box size (see text).

The algorithms used to built 2D composition images were designed with the APHELION software from ADCIS (Caen, France). Fully random to highly regular distributions of solid cells have been generated, in order to simulate different types of solidification structures. In a first step, *(n+2)×(n + 2)* 'solid' seeds (i.e. single pixels) were implemented in a square image of *N(1+2/n)×N(1+2/n)* pixels, set as grey-tone image coded with 256 grey levels (from 0 to 255). Hereafter, this image will be referenced as 'simulation image'. After the generation of the image has been carried out as detailed below, only the inner part of this image of size N×N pixels was considered, giving what will be referenced as 'composition image' below. This procedure was necessary to avoid any bias resulting from border effects. Random structures were realized by implementing *(n+2)×(n+2)* solid seeds at random in the image, following a uniform Poisson process. Non-random structures were obtained by dividing the images in (n+2)×(n + 2) boxes and implementing one solid seed in the central part of each box, as illustrated in Fig. 1. More and more regular patterns were created by decreasing the size L_C of this central part from the size L of the box to a lower value. Perfectly periodic images are obtained when the central part restricts to the central pixel of each box.

After implementation, the (n+2)×(n + 2) seeds were made to grow (i.e. neighbour pixels were attributed to the solid phase) by step-by-step Euclidian dilations with a circle of size one pixel. At each dilation step, the new solid fraction fs was measured within a mask of size N×N corresponding to the area covered by the future composition image. From this measure, the solute content of the solid layer generated in the next dilation step can be calculated using Eq. (1). This growth procedure was repeated until the solid fraction was equal or higher than (1−feut). The eutectic composition was then attributed to all the remaining (non-transformed) pixels. Several images were generated for each set of structure parameters.

Although APHELION software allows working with greytone images coded with real values of composition, we chose to use images in which the grey levels were coded in integer values ranging from G_{min} =1 to G_{max} = 150 for the pro-eutectic solid and equal to 250 for the eutectic phase. The main advantage of this coding convention is to allow using the same composition analysis algorithms (see next paragraph), whatever the solidification model used to generate the images. This required

to convert the solute content ω^s of the proeutectic solid in a grey level G = Aω^s + B, where A and B are constants calculated as

$$A = (G_{\max} - G_{\min})k^{-1}(w^{\text{eut}} - w^0)^{-1} \quad \text{and}$$
$$B = G_{\min} - Akw^0 \tag{2}$$

For the binary system treated in the present study, A = 30.223 and B =−19.552. It is worthwhile to note that the precision loss due to real-to-integer conversion is low with regard to the precision of composition measurement. Indeed, in our case the sampling in 150 levels of compositions ranging from kω^0 = 0.0068 to kω^{eut} = 0.0561 corresponds to a composition resolution of about 4×10−4, that is much lower than the resolution of EDS or WDS techniques.

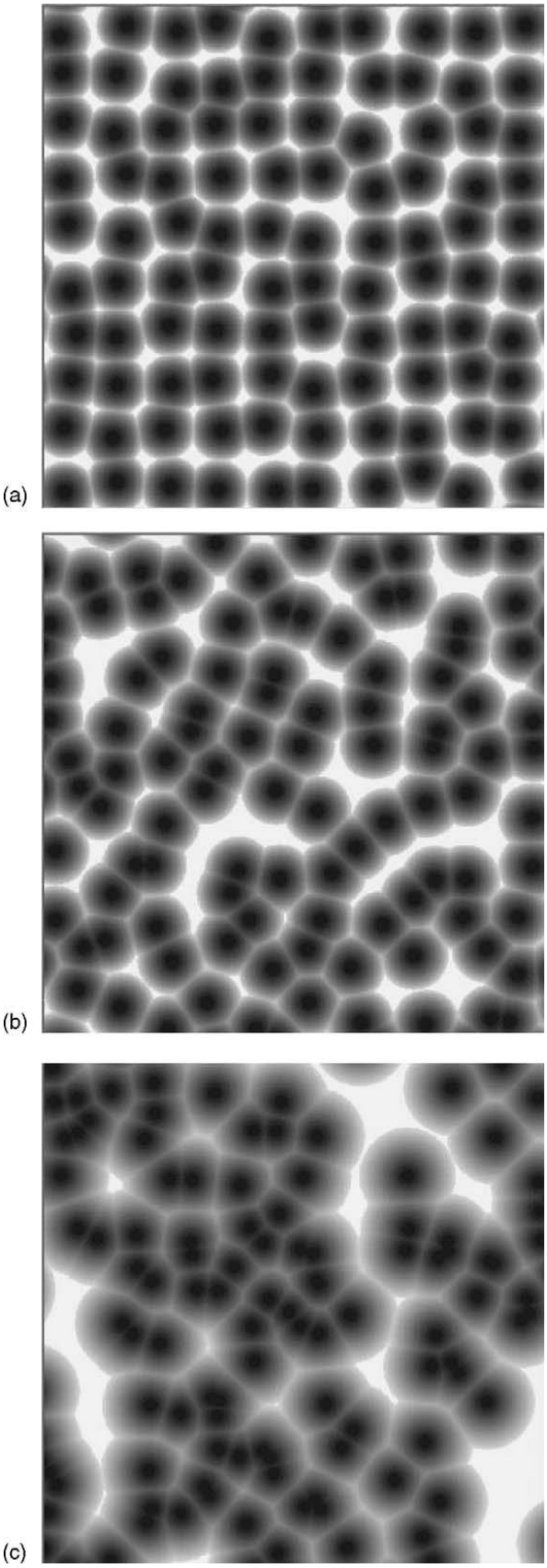

Fig. 2. Examples of images generated with 12×12 seeds implemented with constraints (a: L_C/L = 0.4; b: L_C/L = 0.9) or at random (image c). After generation, the boundary of the images was withdrawn to avoid any border effect (see text). For better illustration, the grey scale of the images has been changed from linear to logarithmic.

Fig. 2 shows examples of composition images 1000×1000 pixels in size obtained with n = 10. Images a and b correspond to LC/L equal to 0.4 and 0.9, respectively, image c relates to a random implementation. Fig. 3a shows the comparison of grey level cumulative distribution associated with three different semiregular images of Fig. 2b type. These distributions (which will be called composition profiles afterwards) appeared to be similar for the three images, indicating that the ratio between image size and cell density was appropriate. Fig. 3b shows the comparison of four composition profiles measured for one perfectly periodic image and one image of each three types illustrated in Fig. 2. Once again, these compositions are superimposed, indicating that the different generation algorithms did not introduce significant bias with respect to the reference composition profile.

3. "Chemical analysis" of the images

Different algorithms were developed to simulate the procedure of chemical analysis, either along a regular square grid or by random sampling over the composition image. As the typical scale of solidification structures is several tens of micrometers while the usual diameter of microprobe spots is about 1 m, it is reasonable to consider the grey level associated with one pixel in one 1000×1000 image as representative of the experimental composition, if neglecting the bias related to the measurement technique. Thus, simulation of a spot analysis is equivalent to a sub-sampling over the composition images. Square grid sampling was simulated by picking up the values of P×P pixels separated by a distance L (in pixels too), while an equivalent random sampling was obtained by picking up P2 pixels selected in the image through a uniform random process.

It is expected that the composition profiles obtained by picking up values on non-random images using a regular grid would be biased when the step of the grid equals the size of the box (or in other words the average or apparent wavelength of the microstructure). To illustrate this, a regular grid of M=10×10 measurement points was implemented with the first point located on the diagonal of the first box, at coordinates (given in pixel number) successively set to (0, 0), (10, 10), (20, 20), (30, 30), (40, 40) and (50, 50), the latter position corresponding to the centre of the first box (see Fig. 1). Fig. 4a and b compares the composition profiles thus obtained on two non-random images, with LC/L, respectively, equal to 0.4 and 0.9, with the reference profile corresponding to the whole images shown with solid line.

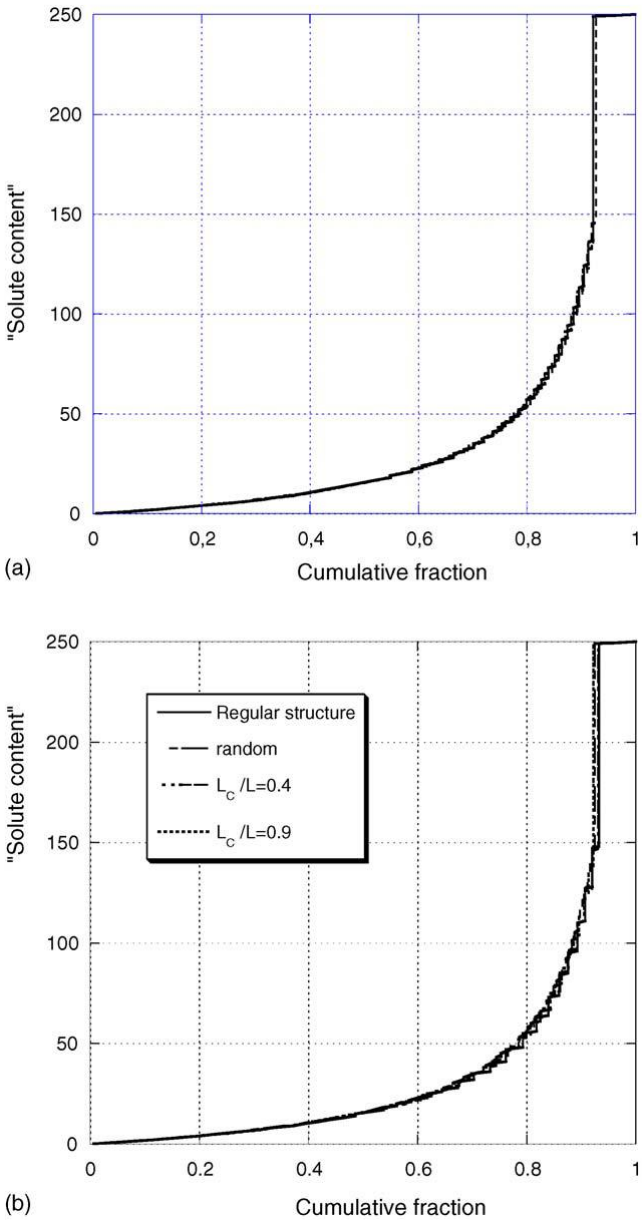

Fig. 3. (a) Composition profiles obtained on three images of the type Fig. 2b, plotted as grey level vs. cumulative fraction of points (i.e. the number of pixels having a grey level lower than a given value divided by the total number of pixels of the image). (b) Comparison of the composition profiles obtained on one of the three types of images shown in Fig. 2 and on one regular image.

As the position of the starting point moves from the corner of the box to its centre, the apparent fraction of eutectic decreases and the composition profiles shifts to higher value of the cumulative fraction. As can be seen when comparing Fig. 4a–b, this effect is stronger the higher the structuring of the image.

4. Discussion

Solute distributions can also be arranged in classes for statistical analysis as proposed by Gungor [8] who used six classes to sort 300 measurement points in the case of (Al) primary phase of a Al–4.5% Cu alloy. This is equivalent to a partitioning of the material in sub-phases with a volume fraction estimated as $V_j^* = V_j/P^2$, where P_j is the number of measurement points falling in class j and P^2 is the total number of measurement points. The variance of the maximum likelihood estimate of volume fraction V_j^* of sub-phase j used by Gungor was expressed as $Var\left(V_j^*\right) = V_j/P^2$, following an

analysis proposed by Hilliard and Cahn [10] under the assumption of small value of V_j and of a sampling grid coarse enough so that there was no correlation between two successive measurement points. Note that without the first assumption, Var (V_j^*) is simply equal to $V_j\left(1-V_j\right)/P^2$, which is the variance of a binomial distribution. When the grid is not coarse enough, or when its periodicity interferes with a wavelength inherent to the microstructure, correlation may show up as was illustrated in Fig. 4. In such cases, a classical statistic analysis of experimental data can evidently give biased estimations, leading to wrongly reject a distribution model. For instance, for the data represented in Fig. 4, the variance of the eutectic fraction estimated from 100 measurement points should be 7.4×10^{-4}, leading to a standard deviation of about 3%. It is seen in this figure that the variations of the eutectic fraction from one distribution to another may be much higher than this value in the case of a non-random structure. This can also occur if the grid is not coarse enough. To avoid this bias, it may appear more appropriate to use a random implementation of the measurement points as previously done by a few authors [9,11,12]. Hilliard and Cahn [10] showed that this choice is associated with an increase of the measurement uncertainty; the variance of estimation of area fractions is increased by an additive term related to the fact that a random point process can never ensure that all points are uncorrelated.

However, most micro-analysers only allow regular grids to be computed. The periodicity and the large scale of solidification structures lead to suspect that there is no minimal grid size value over which it can be ensured that no bias will be introduced by sampling. However, it may be possible that exists a value of the ratio between the characteristic size of the solidification microstructure and grid step size minimizing this bias.

From the above analysis, a procedure for the determination of chemical composition distribution through spot analysis may be suggested. The first step will be to evaluate the characteristic distance over which correlations exist, the so-called range of the image. It is very often possible to obtain an image of the area to be analysed, through light or electronic microscopy. It can also often be assumed that the grey tones of this image are related to the local chemical compositions, thought not necessarily in a linear manner (if it would be the case, the time consuming chemical analysis would not be necessary!). It should be noted however that the case where the variation is not monotonous is out of the scope of this paper. Such an image can be used to evaluate the range of the microstructure through an appropriate statistic approach such as the variogram function. More details on this powerful statistic tool can be found elsewhere (for instance in [13]). In case of a grey-tone image I, the variogram γ(I, h), where h is a translation vector between pixels, is measured as

$$\gamma(I,\vec{h}) = \frac{1}{2}\frac{\sum_{N_{\vec{h}}}[G(x)-G(x+\vec{h})]^2}{N_{\vec{h}}}$$

where G(x) and G(x + $\vec{h}$) are grey-tone values of a couple of pixels separated by $\vec{h}$ and $N_{\vec{h}}$ is the number of couples available in the image. In case of an anisotropic microstructure, the variogram should be recorded in various directions and the largest range should be considered.

To illustrate the approach, we now considered the different simulated composition images discussed before as grey-tones images and calculated their variogram function along the horizontal axis. Fig. 5 shows the evolution of $\gamma(I,\vec{h})$ versus $\|\vec{h}\|$ for different types of structures. It can be seen that the variogram function stabilises around an asymptote in the case of random structures, while more or less marked oscillations appear when some periodicity exists in the composition image. When dealing with real microstructures, we propose that the strategy to adopt for chemical analysis will

depend on the evolution of the experimental variogram. If it stabilises rapidly, i.e. for a range rather small as compared with the size of the scanned region, the best procedure consists to choose a regular point grid analysis with a grid step larger than this range. In such a case, the measurement points are uncorrelated and the classical tools for statistical analysis can be used. For instance, the variance of estimation of the volume fraction of a phase X (eutectic phase or regions within a given composition class) is obtained as $\mathrm{Var}\left(V_j^*\right) = V_j\left(1 - V_j\right)/P^2$. If the variogram does not stabilise over the scanned distance or if it does so at a distance which is too large to allow for a statistically pertinent grid analysis over the available region of interest, two strategies can be used: (i) a random point analysis, which requires to be able to control the stage displacement software and which is probably also more time consuming than a regular grid analysis; (ii) a regular "fine" grid analysis. In this latter case, a Khi-2 analysis to be published elsewhere shows that the optimum grid step size would likely be equal to $D_V(p+1/P)$, where D_V is the distance of the first minimum on the variogram curve (along x or y), P is the number of grid points along x- or y-axis, and p is an integer chosen to explore the largest region as possible. Whatever the procedure, the variance of estimation will be larger than in the uncorrelated case and will depend on the ratio of the variogram range over number of solidification cells.

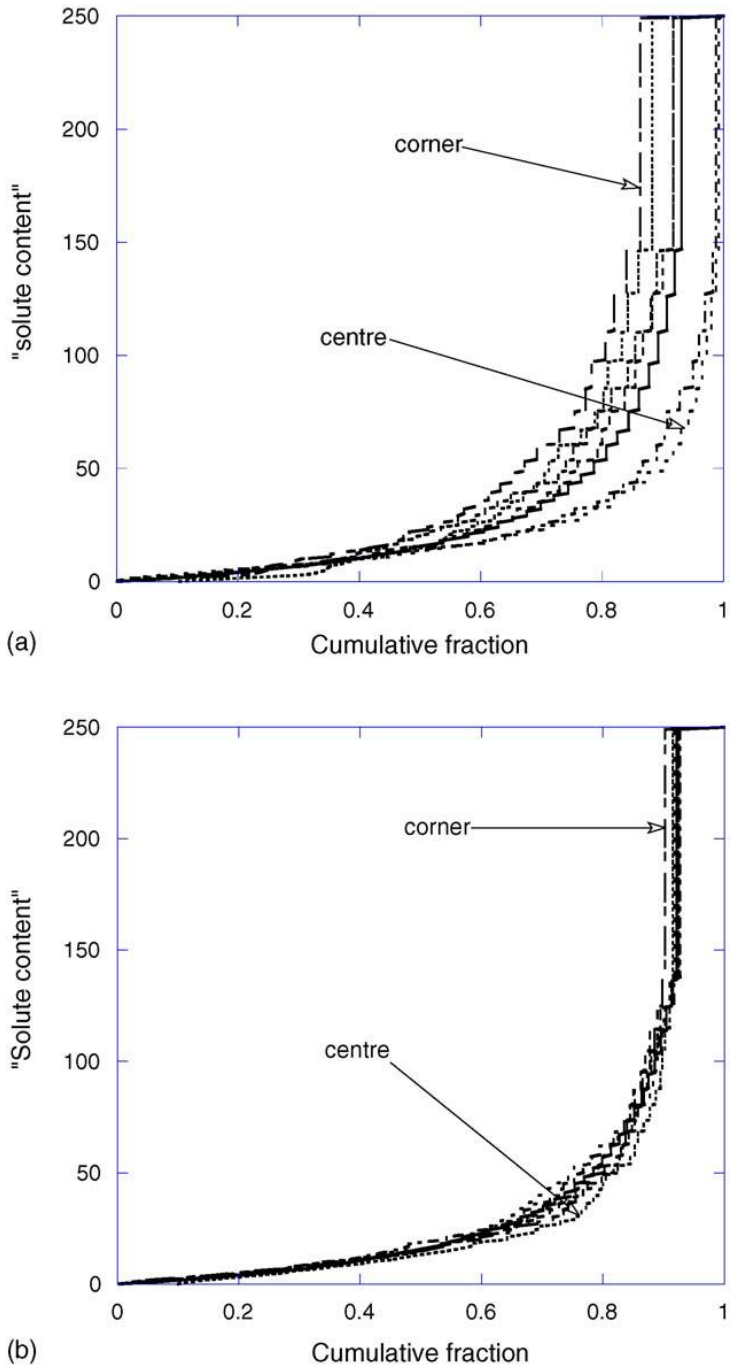

Fig. 4. Comparison of the composition profiles obtained from points on a regular grid compared to the whole distribution shown with solid lines: (a) image made with LC/L = 0.4; (b) image made with LC/L = 0.9. The grid had a step equal to the size of the box and started at points located between the corner and the centre of the first box (see Fig. 1).

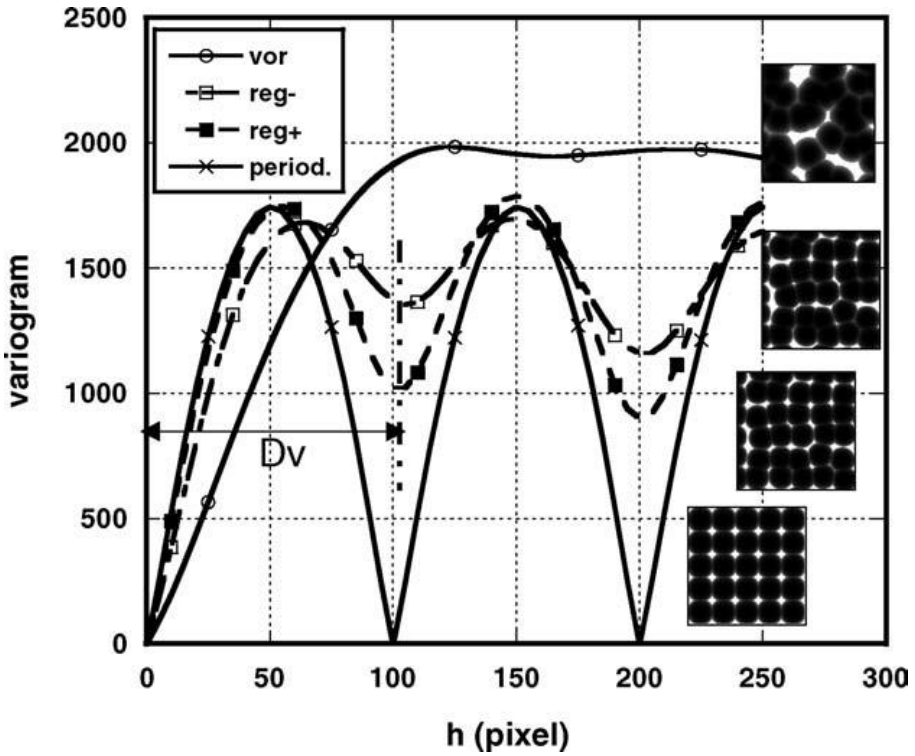

Fig. 5. Evolution of the variogram function γ(I, h) vs. || h||, for different types of microstructures (illustrated on the right side) and denoted vor, reg−, reg+ and period from the less to the more regular one.

5. Conclusion

The above analysis gives hints on how to characterize chemical heterogeneities by means of point counting. Emphasis was put on the fact that statistically significant procedures may differ, depending on the ratio between the characteristic distance of the heterogeneities under investigation and the size of the scanned area. Whilst this analysis was illustrated on simulated images, there are a number of complicating features in case of actual analysis which should be investigated further. In the above analysis, itwas assumed that measurements are not biased, while actual counting may be biased in several ways. For example, measurements made on multi-phase areas (e.g. eutectic) or close to a phase interface will certainly not give significant estimates. Such a bias may be easily circumvented in the case of a monotonous evolution of the composition with solid fraction.

On the contrary, analysis of data on multi-phase material with non monotonous change of the solid composition should need further assumptions. The physical noise associated with X-ray emission may also lead to part of the data being sorted in a wrong class. This has been shown to be one good reason for the negative curvature at low solid fraction on the curves composition versus solid fraction [14], thought variation in the size of the microstructure is also expected to lead to a similar effect when solid state back diffusion is not negligible [15]. Both of these effects could be easily studied on images simulated as in the present study and then appropriately modified.

References

[1] J.A. Sarreal, G.J. Abbaschian, Metall. Trans. 17A (1986) 2063–2073.

[2] J. Lacaze, G. Lesoult, in: J.A. Sekhar, J. Dantzig (Eds.), Nature and Properties of Semi-solid Materials, TMS, Warrendale, PA, USA, 1991,pp. 105–141.

[3] M. Drouzy, C. Mascré, Mem. Et. Sci. Rev. Metall. 58 (1961) 241–260.

[4] M.C. Flemings, Solidification Processing, McGraw-Hill, New York,1974.

[5] T. Grosdidier, A. Hazotte, A. Simon, High Temperature Materials for Power Engineering 1990, Kluwer Academic Publishers, 1990, p. 1271.

[6] W. Hermann, J. Lacaze, D. Oquab, Adv. Eng. Mater. 5 (2003) 32–37.

[7] E.A. Feest, R.D. Doherty, Solidification Technology in the Foundry and Casthouse, The Institute of Metals, London, 1983, pp. 188–194.

[8] M.N. Gungor, Metall. Trans. 20A (1989) 2529–2533.

[9] W. Yang, W. Chen, K.-M. Chang, S. Mannan, J. DeBarbadillo, Metall. Mater. Trans. 31A (2000) 2569–2574.

[10] J.E. Hilliard, J.W. Cahn, Trans. AIME 221 (1961) 344–352.

[11] A. Lendvai-Ny´eki, V. Sapsal, V. Strefaniay, Proceedings of the Seventh International Light Metals Congress, 1981, pp. 64–65.

[12] M.A. Martorano, J.D. Trani Capochi, Metall. Mater. Trans. 31A (2000) 3137–3148.

[13] J. Serra, Image Analysis and Mathematical Morphology, Academic Press, London, 1982.

[14] J. Lacaze, G. Lesoult, ISIJ Int. 35 (1995) 658–664.

[15] J. Lacaze, P. Benigni, A. Howe, Adv. Eng. Mater. 5 (2003) 37–46.